Fabrication and characterization of SMA hybrid composites

Travis L. Turner*, Cynthia L. Lach**, Roberto J. Cano***
NASA Langley Research Center

ABSTRACT

Results from an effort to fabrication shape memory alloy hybrid composite (SMAHC) test specimens and characterize the material system are presented in this study. The SMAHC specimens are conventional composite structures with an embedded SMA constituent. The fabrication and characterization work was undertaken to better understand the mechanics of the material system, address fabrication issues cited in the literature, and provide specimens for experimental validation of a recently developed thermomechanical model for SMAHC structures. Processes and hardware developed for fabrication of the SMAHC specimens are described. Fabrication of a SMAHC laminate with quasi-isotropic lamination and ribbon-type Nitinol actuators embedded in the 0° layers is presented. Beam specimens are machined from the laminate and are the focus of recent work, but the processes and hardware are readily extensible to more practical structures. Results of thermomechanical property testing on the composite matrix and Nitinol ribbon are presented. Test results from the Nitinol include stress-strain behavior, modulus versus temperature, and constrained recovery stress versus temperature and thermal cycle. Complex thermomechanical behaviors of the Nitinol and composite matrix are demonstrated, which have significant implications for modeling of SMAHC structures.

Keywords: Shape memory alloys, Nitinol, embedded actuators, hybrid composites, nonlinear thermoelasticity, composite fabrication, thermomechanical characterization

1. INTRODUCTION

Shape memory alloys are a class of materials that exhibit a martensitic transformation when cooled from the higher-temperature austenitic state. The interaction of temperature and applied stress in driving the martensitic and reverse transformations can be used to exploit phenomena such as the shape memory effect (SME) and pseudo-elasticity. The SME can be described in simple terms in the following manner. A SMA can be easily deformed in the low temperature martensitic condition and can be returned to its original configuration by heating through the reverse transformation temperature range. Conversely, a large tensile stress can be induced if the SMA is prevented from recovering the deformation. Extensive work has been done to characterize the microstructure and properties of these materials[1,2]. Compilations of papers have also been published[3-6], which give a good overview of the characteristics of SMAs and their applications. Birman[7] gave a comprehensive review of work done in the areas of alloy characterization, constitutive modeling, and applications.

Shape memory alloys have been investigated for a variety of applications since their discovery. A new class of applications was developed when Rogers and Robertshaw[8] introduced the idea of embedding SMA actuators in a composite laminate for structural control. A structure of this type has been termed a shape memory alloy hybrid composite (SMAHC). Paine and Rogers published a review of SMAHCs and their applications[9]. Two methods have been proposed for integrating SMA actuators into a composite; bonding the actuators within the composite matrix as a constituent and embedding the actuators within sleeves through the laminate. The work presented in this study focuses on the former method, where prestrained actuators are bonded within the composite matrix and the boundaries of the structure serve also as mechanical restraints for the actuators. Thus, an inherently elevated thermal environment in service will activate the actuators, which act against the mechanical boundaries to adaptively stiffen the structure without control electronics or auxiliary power.

A thermomechanical model was recently developed to study the static and dynamic response of SMAHC structures[10-12]. The model captures the thermal nonlinearity of the SMA and composite matrix, but is macromechanical in nature such that it depends only upon measurement of fundamental engineering properties. The goals of the work presented in this paper are to present a robust fabrication process for reliable SMAHC specimens and characterize the thermomechanical properties of the

* t.l.turner@larc.nasa.gov; phone 757 864-3598; fax 757 864-8823; Structural Acoustics Branch, Mail Stop 463, Hampton, VA 23681-2199; ** c.l.lach@larc.nasa.gov; phone 757 864-3133; fax 757 864-7893; Metal and Thermal Structures Branch; Mail Stop 188A; *** r.j.cano@larc.nasa.gov; phone 757 864-3951; fax 757 864-8312; Advanced Materials and Processing Branch, Mail Stop 226

SPIE 8th Annual International Symposium on Smart Structures and Materials; Active Materials: Behavior and Mechanics, C. S. Lynch (Editor), SPIE Vol. 4333, Paper No. 4333-60, Newport Beach, CA, 4-8 March 2001.

constituent materials. Hardware and processes for overcoming practical fabrication issues are discussed. Results from the thermomechanical testing demonstrate the complex thermoelastic nature of the material system and stress the importance of accurate characterization to enable SMAHC performance prediction. Results from static and dynamic tests performed on the SMAHC specimens and validation of the thermomechanical model are given in related publications[10,11,13].

2. BACKGROUND

In the typical application being considered, such as adaptive stiffening of aerospace structures, the SMA elements would be activated through an inherently elevated temperature of the service environment. This effect can be simulated in experiments by various means, of which the most practical is resistive heating. Resistive heating has the advantages of simple operation, relatively uniform heating, and excellent controllability. A glass-epoxy matrix material system was selected to avoid any potential electrical conduction problems. This material system also affords the advantage of visual flaw detection due to its translucency. A Nitinol alloy was selected because of favorable electrical resistance, availability, and shape memory capabilities.

Glass-epoxy unidirectional prepreg tape was obtained from Fiberite, Inc. The material is Hye 8 End/934, an E-glass/934 epoxy resin material system. The resin material is formulated for autoclave processing and the following cure procedure is recommended; heat at 1.1–2.8°C/minute (2–5°F/minute) to 121.1°C (250°F) and hold for 15 minutes, apply 689.5 kPa (100 psig) pressure and continue to hold at 121.1°C (250°F) for an additional 45 minutes, heat at 1.1–2.8°C/minute (2–5°F/minute) to 176.7°C (350°F) and hold for 120 minutes, and cool at 2.8°C/minute (5°F/minute) (maximum) to ambient.

A Nitinol alloy in a ribbon form was selected, in lieu of a wire form, as the actuator material in this study to simplify the fabrication procedure, allow for more flexibility in fabrication, and desensitize the actuators to interface voids and stress concentrations. This approach was adopted because recent SMAHC fabrication efforts involving wire-type actuators have suffered from various disadvantages. These disadvantages include complicated fabrication procedures because of the relatively large number of actuators usually needed, sensitivity to actuator/matrix interface flaws because voids can be of significant relative size, and relatively high rate of actuator breakage during cure because of sensitivity to stress concentrations at the mechanical restraints. Finally, it is difficult to achieve a desirable overall volume fraction of SMA in wire form when trying to optimize the integration of the actuators by placing them in only selected layers. Conversely, ribbon-type SMA elements can be placed in strips cut out of particular matrix laminae to result in a rather simple lay-up operation, while keeping the volume fraction high in the desired locations.

A Nitinol alloy was specified with an appropriate composition to give a martensite finish temperature above the expected ambient temperature while maintaining an austenite finish temperature well below the glass-transition temperature of the Fiberite 934 epoxy matrix (193.3°C, 380°F). Shape Memory Applications, Inc. provided the Nitinol ribbon material with nominal transformation temperatures, in a fully annealed state, of A_s=67°C, A_f=85°C, M_s=46°C, and M_f=32°C. These temperatures were reportedly determined by differential scanning calorimetry (DSC). For basic material characterization and to determine the condition of the alloy in the as-received state, both DSC and direct current plasma (DCP) emission spectroscopy were performed at NASA LaRC.

Small samples (<10mg) were cut from the ribbon material in the as-received condition for the DSC testing. Scans were performed at a rate of 5°C/minute with the following procedure; heat from ambient temperature to 150°C (first heat), cool from 150°C to –20°C, and repeat this entire profile once the sample was returned to ambient from –20°C (second heat). Representative results from the DSC tests are shown in Figure 1. The shape of the first-heat endotherms were ill behaved and not repeatable, while the analogous second-heat endotherms were repeatable. This effect is attributable to first-heat recovery of the mechanical deformation induced during packaging the ribbon on a spool and/or shearing the small samples needed for DSC measurements from longer lengths.

Note that the DSC signature shows two distinct exothermic peaks during the cooling portion of the cycles; one peaking at approximately 39°C and attributable to the R-phase transformation, the other peaking at approximately 9°C due to the usual twinned martensitic transformation. The R-phase is a by-product of a partially annealed condition and does not adversely affect performance[6]. Thus, the transformation temperatures for the Nitinol in the as-received condition and in a free configuration are approximately A_s=45°C (113°F), A_f=60°C (140°F), M_s=17°C (62.6°F), and M_f=0°C (32°F). The start and finish temperatures indicated here mark the onset/termination of substantial phase transformation activity. However, measurable activity can be seen in the tails of the exothermic and endothermic peaks of the DSC signatures. Also note that

the martensitic transformation of the alloy in this state resides completely below ambient temperature. These observations will be revisited in the next section.

The Nitinol alloy was analyzed for nickel, titanium, and iron content by DCP analysis, as referenced in ASTM E1097-97. After sample preparation, duplicate 0.1 g samples were dissolved in a mixture of hydrofluoric and nitric acids. Once dissolution was complete, the samples were diluted to a specified volume and analyzed for the above elements by DCP analysis using matrix-matched calibration standards. Duplicate samples were prepared and analyzed for oxygen and nitrogen by inert gas fusion, as referenced in ASTM E1019-00. The average results of the analyses reported in weight percent are 55.4Ni-44.3Ti-0.033C-0.1965O-0.0011H-0.0075N-0.0075Fe; wt%.

For simplicity, a beam-type specimen is the focus of this study, but all discussion and results are directly extensible to more practical configurations. A schematic of the selected beam-type specimen is shown in Figure 2. Various constraints, other than the use of ribbon-type actuators, influenced the design of this laminate. These constraints include fabrication tooling geometry and dynamic range of anticipated experimental configurations. The specimen design is by no means optimized, but the predicted performance is in a range that is suitable for the expected loading conditions and to demonstrate significant improvement from the SMA reinforcement.

Note that this specimen design calls for a quasi-isotropic lamination $(45/0/-45/90)_{2s}$ with a SMA actuator cross section of 0.0127x1.27e-4 m (0.5x0.005 inches) to be embedded within each 0° glass-epoxy layer, i.e., replace a portion of each 0° layer. Material availability and processing limitations dictated a nominal cross section of 0.0023x1.5e-4 m (0.09x0.006 inches). This thickness was considered acceptably close to the estimated glass-epoxy unidirectional tape thickness (1.27e-4 m, 0.005 inches) and it was planned that five widths of the ribbon would be placed side-by-side to develop a width near that in the specimen design.

3. SPECIMEN FABRICATION

The SMAHC specimen fabrication procedure used in this study consists of the following steps; prestrain (elongate) the SMA actuators, lay-up the composite laminate, cure the laminate while restraining the actuators, and machine beam specimens from the consolidated SMAHC laminate. The Nitinol material was packaged on a spool, which subjected the ribbon to significant out-of-plane bending strain. Significant axial and some in-plane bending and torsional strain were also imparted to the ribbon during the spooling operation. This packaging strain must be removed prior to imparting the actuator prestrain. The packaging strain can be conveniently recovered by inducing the reverse (austenitic) transformation by heating from ambient temperature to ~100°C (~200°F), as shown in Figure 1. An apparatus was developed to perform this operation by resistive heating, shown in Figure 3. The apparatus consists of an electrically insulating board with a dovetail track within which brass electrical blocks can slide freely. Ribbon lengths are installed in the brass grips and subjected to resistive heating by DC electrical current at a level known to induce the desired temperature over the length of the ribbon, while preventing the electrical connections from inducing additional undesirable deformation or significantly loading the specimen.

It is desirable to induce the martensitic transformation just prior to prestraining in order to avoid aging effects, such as the rubber-like form of pseudoelasticity[6]. Inducing the transformation can be accomplished during the packaging strain recovery process as the ribbon cools from ~100°C (~200°F) to ambient temperature. It was shown in the previous section that, for this particular Nitinol composition in an unrestrained condition, the martensitic transformation is not complete at ambient temperature. However, the martensite can be stress-induced during the prestraining operation. Stress-inducing the martensite results in essentially the same state as would be achieved by cooling the ribbon to sub-ambient temperatures to complete the martensitic transformation prior to prestraining. The main difference is that there may be some austenite remaining in the ribbon after prestraining by the former method, but should be of no consequence because any subsequent thermal cycling (e.g., composite cure) will render the state from the two methods equivalent. The former method, without cooling to sub-ambient temperatures, was selected for simplicity.

The prestraining operation needs to be very precise and repeatable because the actuator performance is a very strong function of prestrain level. This was accomplished by elongating the actuators on a servohydraulic test machine operated in stroke-control mode. Alignment of the ribbon during elongation is critical to avoid bending strain and to obtain repeatable results. Handling of the ribbon is cumbersome during installation in the test machine, and it is desirable to prestrain multiple strands at once to expedite the process. In order to rectify these issues, an apparatus was developed to align and maintain proper geometry on three ribbon lengths at once during installation in the test machine. A close-up view of the alignment/gripping apparatus is shown in Figure 4. The entire assembly (alignment/gripping apparatus, spacer, and three ribbons) is shown

installed in the test machine in the left half of Figure 5. The Nitinol ribbons are shown ready for elongation, subsequent to spacer removal, in the right half of Figure 5.

The particular spacer length shown was used to maintain a SMA ribbon gage-length of 0.635 m (25 inches) for manufacture of the beam specimens shown in Figure 2. The gage length of the ribbons was elongated to a length of 0.6604 m (26 inches), which corresponds to a prestrain of 4%. This gage length was used in order to ensure uniform prestrain over the 0.6604 m (26 inch) span between mechanical restraints on the composite lay-up tooling plate, which will be discussed subsequently. Cross-section dimension measurements were made at 0.0254 m (1 inch) intervals on a representative prestrained ribbon. The average cross section of the ribbon was determined to be 2.26x1.63e-4 m (0.089x0.0064 inches) for an average area of 3.67e-7 m^2 (0.00057 in^2). This average area was used in all of the stress calculations shown later in this document.

A mechanical drawing of the lay-up and cure tooling plate is shown in Figure 6. This apparatus was designed to provide a flat surface (±0.005 inches) and mechanical grips to restrain the SMA during an autoclave cure procedure. Recall that the beam specimen design calls for a lamination of $(45/0/-45/90)_{2s}$ with the Nitinol in the 0° layers. This lamination was accomplished by cutting widths of the 0° layers to size during assembly and filling the void with five ribbon widths laid side-by-side. A picture of the lay-up procedure at the stage of finishing the first 0° layer is shown in Figure 7. Note that Kapton release film, fiberglass breather cloth, and teflon-coated fiberglass bleeder cloth are layered between the tooling plate surface and the first glass-epoxy layer, in that order.

The laminate after complete assembly is shown in Figure 8, where it can be seen that cure cycle control thermocouples have been installed near the laminate and the Nitinol ribbon ends have been secured within the knurled mechanical restraints. The restraints consisted of three parts; the tooling plate surface, a thin spacer with knurling on both sides, and the top clamping bar. This arrangement was employed to minimize bending of the actuators between the laminate boundary and the restraint and to maximize grip for each layer of SMA by minimizing the number of layers gripped together. The mechanical restraint screws received a torque of 11.30 N·m (100 in·lbf). The release paper was subsequently removed from the top layer of glass-epoxy and the laminate was topped with bleeder cloth, Kapton film, a caul plate, bleeder cloth, and breather cloth, in that order. The entire assembly was vacuum bagged and drawn to an internal pressure of 0.0475 atm.

The assembly was subjected to the autoclave cure cycle recommended by the vendor (Fiberite, Inc.) and the resulting consolidated part is shown in Figure 9. Two SMAHC beam specimens were machined from this laminate using the respective centerlines of the embedded Nitinol ribbon. The beam specimens are shown in Figure 10, where it can be seen that one beam has been prepared for installation in test fixtures. The beams have dimensions of 0.5588x0.0254x0.0019 m (22x1x0.078 in). The SMA leads of the test-prepared beam were trimmed to an overall length of 0.6604 m (26 in). The overall volume fraction of the SMA within the glass-epoxy dimensions is approximately 13.8%.

4. MATERIAL SYSTEM CHARACTERIZATION

The material system and processes used to fabricate SMAHC beam specimens were described in the previous sections. In order to predict the thermomechanical behavior of such a structure using the previously mentioned model[10-12], a number of material properties from the constituents must be determined. Results from characterization tests performed on the glass-epoxy matrix material and Nitinol alloy are described in the following subsections.

4.1 Glass-Epoxy Thermomechanical Properties

Two laminates were fabricated from the glass-epoxy material system to provide specimens for thermomechanical testing; a unidirectional lay-up $(0)_{20}$ and an angle-ply lay-up $\pm(45)_4$. Tab material was post-cured to the laminates and the resulting structures were machined into uniaxial tensile specimens with dimensions of 0.2286x0.0254 m (9x1 inches) (gage length of 0.1524 m, 6 inches). The tensile specimens were instrumented with a "T-strain gage" at the mid-span and tested on a servo-hydraulic test machine. The unidirectional specimens were tested according to ASTM D3039-95a for estimates of the Young's moduli and Poisson's ratios; E_1, E_2, ν_{12} and ν_{21}. The angle-ply specimens were tested according to ASTM D3518-94$^{\varepsilon 1}$ for estimates of the shear modulus G_{12}. Although the ASTM standards call for modulus estimates to the determined over strain ranges of ~1000–3000 με and ~2000–6000 με, respectively, the transverse (90°) uniaxial and ±45° angle-ply stress-strain relations showed discernible nonlinearity over those ranges. The maximum normal strain and shear strain for the test configurations considered for this material system are not expected to exceed 500 and 250 με, respectively. Therefore, E_2

and G_{12} estimates were determined from ~50–1000 με and ~50–500 με strain ranges, respectively, to achieve estimates more representative of the intended configurations.

Specimens for measurement of the coefficient of thermal expansion (CTE) were also machined from the unidirectional laminate $(0)_{20}$ described above and tested by two different methods; ASTM E228-95 and an interferometric dilatometer method. Both quadratic and cubic interpolation of the raw thermal expansion data are used in practice to generate linear and quadratic estimates of the CTE with temperature, respectively. Cubic interpolation was employed with the ASTM E228-95 method while quadratic interpolation was used with the interferometer method. The two methods were in agreement for the overall trend in the CTE data, but the cubic interpolation of the data collected with the ASTM standard captured significant higher order effects, which may be important for thermomechanical modeling.

A summary of the glass-epoxy thermomechanical properties is shown in Table 1. The tabulated CTE data are from the ASTM E228-95 method.

4.2 Nitinol Thermomechanical Properties

Data pertaining to the material property and performance characteristics of the Nitinol alloy were acquired through thermomechanical testing performed at Lockheed Martin Astronautics (LMA) and at NASA LaRC. Although rigorous training could have been performed on the alloy to generate a thermomechanically stable actuator material, the elevated cure temperature of the glass-epoxy matrix material (176.7°C, 350°F) was considered to be high enough to risk degrading the expensive training. Thus, thermomechanical testing was performed to quantify the material characteristics as a function of thermal cycle. Two types of tests were performed; measurement of recovery force versus temperature at constant prestrain level and measurement of load versus deflection at constant temperature. Discussion will focus on testing performed at LMA first, followed by the testing performed at NASA LaRC.

Tests at LMA were performed on nominal 0.254 m (10 inch) gage lengths of the ribbon material. Recovery force tests were performed to measure the maximum recovery force generated by the actuator material as a function of thermal cycle and initial strain. Each sample was installed in a test rig, elongated a predetermined amount (2%, 3%, or 4%), and immediately tested. The recovery force was normalized to the average cross-sectional area of the prestrained ribbon to result in recovery stress. The results of these tests are shown in Figure 11, indicated in the legend by LMA. It can be seen that in all cases the maximum recovery stress diminishes rapidly out to about 10 thermal cycles and approaches an asymptotic value at about 50 cycles. Additional tests were performed with the 2% and 4% prestrain samples after the thermal cycling tests to measure the variation of the stabilized recovery force with temperature. These tests constituted thermal cycle number 51 on those samples and results are presented in Figure 12. Note that the recovery stress starts to increase at a temperature very near ambient (24°C, 75°F). This phenomenon appears to be in disagreement with the DSC results, but closer inspection reveals that it is not. The initial increase in the recovery force is associated with the transformation activity in the low-temperature "tail", below the so-called A_s, of the exothermic peak in Figure 1. The abrupt change in the slope of the recovery stress vs. temperature curve, near 40°C (104°F), is associated with A_s.

Tests were conducted to measure load versus deflection for all specimens involved in the recovery force tests, as well as a specimen in the as-received condition, at ambient and elevated temperature (120°C, 250°F). Representative plots of the two test conditions for the case of a sample prestrained 3% are shown in Figure 13, indicated in the legend by LMA. Young's modulus estimates at ambient temperature were calculated from only the initial (0–25.5 MPa, 0–3.7 ksi) portion of the ambient temperature stress-strain curve, while the overall slope of the elevated temperature data was used for elevated Young's modulus estimates. Recall that the maximum normal strain is not expected to exceed 500 με in the configurations considered in this study. Therefore, evaluation of the ambient temperature modulus over the small range is considered appropriate. The resulting modulus data and data summarizing the recovery force tests are shown in Table 2.

A couple of options exist, with the available recovery stress data from LMA, for modeling the behavior of the SMA material in the hybrid composite for comparison to experiment. The SMAHC specimens could be thermally cycled enough (e.g., 50 times) to render the structure's properties stable and simply model the SMA recovery stress behavior according to Figure 12. Alternatively, the variation of recovery stress with temperature at each thermal cycle can be estimated from the available data. Construction of such a data set can be accomplished by normalizing the recovery stress versus temperature data at thermal cycle 51 (Figure 12) to the corresponding maximum recovery stress versus thermal cycle data set (Figure 11). Usage

of such a data set allows modeling of the material system without any requirement on thermal cycling of the SMAHC specimens, but has consequences as will be explained subsequently.

The Nitinol recovery stress and modulus data collected at LMA were used, along with the glass-epoxy characterization data, to model the static and dynamic thermomechanical behavior of the SMAHC beam specimens described earlier. The procedure just described was employed to construct the variation of recovery stress with temperature at each thermal cycle. Predicted responses using the LMA data and corresponding measured responses were not in good agreement. A discussion of the reasons for the disagreement follows.

Recall that in the SMAHC specimen fabrication procedures, described in the previous section, the Nitinol ribbon was prestrained 4%. Although data was collected at LMA for this prestrain level, there is a fundamental inconsistency. The ribbon used in the fabrication procedures was necessarily released from tension after prestraining and before embedding in the composite, whereas the recovery force tests at LMA were performed immediately after prestraining and without regripping. Also, the prestrained ribbon that was embedded in the composite specimens was stored in lab conditions for approximately one month prior to embedding. The SMAHC beam specimens were also stored approximately three to six months after cure and before static and dynamic tests. Thus, there was some suspicion that natural aging of the prestrained microstructure may have some effect on the actuator performance. Therefore, additional recovery force and modulus tests were performed at NASA LaRC.

Tests at NASA LaRC were performed on 0.127 m (5 inch) gage lengths of the ribbon with 4% prestrain remaining from specimen fabrication. Three samples were tested; one to 4 thermal cycles and two to 50 thermal cycles. The ribbon had been stored in lab conditions for approximately eleven months between the prestrain process and these characterization tests. An adaptation of the prestraining apparatus was used to configure Nitinol ribbon samples for measurement of recovery force. The ribbon was subjected to a slight preload 4.45 N (1 lbf) to keep the sample taut prior to fixing the test machine grips (stroke control) and exposing the sample to thermal cycling. The ribbon was electrically heated to expedite the thermal cycling process. The recovery force and ribbon temperature at three locations were measured at 2-second intervals during each thermal cycle. The specimen temperature was cycled from ambient to approximately 148.9°C (300°F) over a duration of approximately 15 minutes. The raw data was then processed to estimate the recovery stress with a common temperature resolution and averaged over appropriate samples. The resulting recovery stress versus temperature data corresponding to the second through fourth and the fiftieth thermal cycle are shown in Figure 14. The data for the first thermal cycle are not included, as that information is applicable only to the SMAHC cure cycle. The maximum recovery stress versus thermal cycle (averaged over the two samples cycled 50 times) is shown in comparison to the corresponding LMA data in Figure 11.

It can be seen by comparing the LMA and NASA LaRC data sets (Figures 11 and 14) that the performance of the Nitinol ribbon that was prestrained 4% and released is more similar to that of the 3% prestrain data collected at LMA. Curves analogous to those in Figure 14 were generated from the LMA data by averaging 2% and 4% prestrain data sets in Figure 12 and scaling the resulting load vs. temperature data by the maximum load for 3% prestrain at cycle numbers 2, 3, 4 and 50 in Figure 11. The resulting curves are shown in Figure 15. Note that the 3% prestrain case constructed from the LMA data achieves roughly the same maximum recovery force, but over a much more narrow temperature range. This trend is a real physical phenomenon and may be attributable to natural aging effects or differences in the state of the alloy. Also note the shape change with thermal cycle of the recovery stress vs. temperature curve, evident in Figure 12. This effect is not reflected in the data set constructed from the LMA data and emphasizes the importance of quantifying correctly the recovery stress functionality with temperature vs. thermal cycle.

Tensile tests were conducted in accordance to ASTM E8-00 on the same material with 4% prestrain using 0.127 m (5 inch) gage lengths, with the same gripping apparatus as described previously, to determine estimates of the Young's modulus. The entire assembly, including high-temperature hydraulic grips, was contained within a box furnace. Tests were conducted on 3 ribbon samples at each of 7 temperatures; 21.11°C (70°F), 37.78°C (100°F), 65.56°C (150°F), 79.4°C (175°F), 93.33°C (200°F), 121.1°C (250°F), and 148.9°C (300°F). Estimates from the three samples were averaged and the resulting modulus versus temperature behavior is shown in Figure 16. It can be seen in Figure 13 that the stress-strain behavior was somewhat different from that obtained at LMA, particularly at ambient temperature. These stress-strain differences are reflected in the modulus estimates and appear to be attributable to differences in the state (phase content, thermomechanical history, etc.) of the alloy.

Evidence of the effect of alloy-state differences can be seen in the plot of stress versus strain in Figure 17 for a NASA LaRC ribbon sample with 4% prestrain (reference sample) along with corresponding data from four other samples with varying

types of processing. All samples were tested at ambient temperature and the processed samples include the following; 1) a specimen constrained in the 4% prestrained state and heated to 148.9°C (300°F), 2) a sample with 4% prestrain that was cooled to -18°C (0°F), 3) a sample cooled to -18°C (0°F) prior to imparting the 4% prestain, and 4) a sample that was tested in the as-received state (also for reference). The various treatments were intended to investigate the effect of differences in the phase content (i.e., austenite, twinned martensite, SIM, and R-phase) on the stress-strain behavior. These data indicate that all specimens with 4% prestrain exhibit similar stress-strain behavior, except the sample subjected to the heat cycle under constraint. The latter sample is of a similar state to that of the LMA testing, but the stress-strain data are still not in very good agreement with the LMA data. The reason for this disagreement is not known at this time.

Note that the temperature range over which the modulus exhibits the most variation in Figure 16 (~40°C–80°C) is more narrow than the A_s–A_f range interpreted from Figure 14 (~40°C–100°C). This observation is consistent with the data collected by Cross et al.[1]. The low-temperature transition point is associated with the temperature at which there is significant austenite and high-enough temperature to not allow immediate transformation to martensite upon stress application (~40°C). The high-temperature transition point corresponds to the temperature at which the austenite volume fraction begins to dominate (~80°C).

It is noted that some additional data is needed to fully characterize the Nitinol ribbon. Published data was incorporated for Poisson's ratio (0.3) and the transverse direction CTE for the martensitic 6.6e-6 /°C (3.67e-6 /°F) and austenitic 11e-6 /°C (6.11e-6 /°F) phases as measurement of these properties as a function of temperature would require significant additional effort and development. In light of the previous discussions concerning the differences between the data collected at NASA LaRC and LMA, the data collected at NASA LaRC are more representative of the thermomechanical properties of the Nitinol ribbon actually embedded in the composite. These properties are tabulated in Table 3. Tabulated recovery stress versus temperature data is provided only for thermal cycles 2–4 because those are the important cycle numbers for modeling of the SMAHC specimen behavior reported in a separate paper[13]. Note that the modulus data has been linearly interpolated within the seven measurement temperatures to achieve the more refined temperature resolution. The 2-direction CTE has been interpolated between two transition points noted in regard to Figure 16, 43.33°C (110°F) and 82.22°C (180°F), to approximate the variation within the reverse transformation temperature range. The "in-service" austenite start and finish temperatures, as interpreted from the recovery stress versus temperature data, are 26.7°C (80°F) and 148.9°C (300°F), respectively. However, the temperatures at which the recovery stress vs. temperature curve rapidly changes slope better model the temperature range of property variation, as discussed previously.

The Nitinol characterization data collected at NASA LaRC (Table 3) was used along with the glass-epoxy properties (Table 1) to regenerate predictions of the SMAHC beam specimen performance. The new predictions were in excellent agreement with experimental measurement[10,11,13]. Work is continuing with the Nitinol material to identify potential crystalline aging effects and better understand the relationships between thermomechanical processing, microstructure, and thermomechanical properties.

5. SUMMARY

The main objectives of this work were to develop practical hardware and processes for fabricating reliable shape memory alloy hybrid composite (SMAHC) specimens and to characterize the material system of those specimens to enable numerical predictions of their thermomechanical behavior. A Nitinol alloy in a ribbon form and a glass-epoxy composite matrix were selected for this study. The resulting specimens are intended to demonstrate performance and provide experimental data for analysis validation of adaptive stiffening behavior, which results when the prestrained actuators respond to a thermal excitation in the presence of mechanical constraints at the structural boundaries.

Differential scanning calorimetry (DSC) and direct current plasma (DCP) emission spectroscopy tests were performed on the Nitinol to determine the phase transformation and chemical composition of the alloy in the as-received state. The alloy composition was determined to be 55.4Ni-44.3Ti-0.033C-0.1965O-0.0011H-0.0075N-0.0075Fe; wt%. The characteristic transformation temperatures were estimated at A_s=45°C (113°F), A_f=60°C (140°F), M_s=17°C (62.6°F), and M_f=0°C (32°F). The fact that the martensitic transformation exists completely below ambient temperature is not of significant consequence for the intended application for the specimens.

A SMAHC laminate was manufactured from the glass-epoxy material system with a quasi-isotropic lamination $(45/0/-45/90)_{2s}$ and Nitinol actuators, with a prestrain of 4%, embedded in discrete 0.011 m (0.45 inch) strips in four (0°) of the 16

layers. Beam specimens were machined from the laminate sharing the centerlines of the embedded Nitinol strips. Practical solutions were achieved for overcoming materials processing and various specimen fabrication issues. Such issues include removal of actuator packaging strain, avoidance of rubber-like pseudoelasticity during prestraining, enabling accurate and repeatable actuator prestrain, reducing actuator sensitivity to stress concentrations at mechanical constraints, and enabling strategic actuator placement while maintaining a desirable overall volume fraction.

Tests were performed on the glass-epoxy and Nitinol constituents to determine their thermomechanical properties. The glass-epoxy matrix properties showed significant thermal nonlinearity. The following properties were estimated from the experimental data; E_1, E_2, ν_{12}, G_{12}, α_1, and α_2. The constrained recovery stress behavior of the Nitinol ribbon was measured as a function of temperature, thermal cycle, and prestrain level (2%, 3%, and 4%). Modulus values were estimated from the stress-strain behavior of the specimens used in the recovery stress tests. These initial tests were conducted without releasing the specimen after imparting the prestrain or between the recovery force and tensile tests. Recovery force and tensile tests were also performed on samples of the Nitinol ribbon remaining from the SMAHC specimen fabrication process (4% prestrain). Significant differences were found in the recovery force and stress-strain behavior relative to the initial tests. Effects of natural aging and phase/thermoelastic state differences of the alloy may be contributing to these thermomechanical property differences. Thermal nonlinearity of the Nitinol and composite matrix material, thermal cycle dependence of the Nitinol, and aging/state effects on the Nitinol are all of utmost importance for modeling the behavior of SMAHC specimens.

ACKNOWLEDGEMENTS

The authors gratefully acknowledge the assistance of Craig Ohlhorst (NASA LaRC), William Johnston, Joel Alexa, Stewart Walker, and Harold Claytor (Analytical Services and Materials), Jerry Draper (Lockheed Martin Astronautics), and Kenneth Blount (Materials Research and Engineering) for their help in characterizing the thermomechanical properties of the glass-epoxy and Nitinol materials. Thanks are also due to Scott Wallace (NASA LaRC) and Ravi Shenoy (Analytical Services and Materials) for their assistance in providing differential scanning calorimetry measurements from the Nitinol and Hoa Luong (NASA LaRC) for his help with specimen fabrication.

REFERENCES

1. W. B. Cross, A. H. Kariotis, and F. J. Stimler, "Nitinol Characterization Study," NASA CR-1433, 1969.
2. C. M. Jackson, H. J. Wagner, and R. J. Wasilewski, "55-Nitinol the Alloy with a Memory: Its Physical Metallurgy, Properties, and Applications," NASA SP-5110, 1972.
3. J. Perkins (Editor), *Shape Memory Effects in Alloys*, Plenum Press, New York, NY, 1975.
4. T. W. Duerig, K. N. Melton, D. Stockel, and C. M. Wayman (Editors), *Engineering Aspects of Shape Memory Alloys*, Butterworth-Heinemann, Boston, MA, 1990.
5. H. Funakubo (Editor) (Translated by J. B. Kennedy), *Shape Memory Alloys*, Gordon and Breach Science Publishers, New York, NY, 1987.
6. K. Otsuka and C. M. Wayman (Editors), *Shape Memory Materials*, Cambridge University Press, Cambridge, UK, 1998.
7. V. Birman, "Review of Mechanics of Shape Memory Alloy Structures," *Appl. Mech. Rev.*, **50(11)**, 629-645, 1997.
8. C. A. Rogers and H. H. Robertshaw, "Shape Memory Alloy Reinforced Composites," Engineering Science Preprints 25, Society of Engineering Science, Inc., ESP25.8027, 1988.
9. J. S. N. Paine and C. A. Rogers, "Review of Multi-Functional SMA Hybrid Composite Materials and their Applications," *Adaptive Structures and Composite Materials: Analysis and Application*, **AD-Vol. 45/MD-Vol. 54**, 37-45, ASME, 1994.
10. T. L. Turner, "Thermomechanical Response of Shape Memory Alloy Hybrid Composites," Ph.D. Dissertation, Virginia Polytechnic Institute and State University, 2000.
11. T. L. Turner, "Thermomechanical Response of Shape Memory Alloy Hybrid Composites," NASA/TM-2001-210656, 2001.
12. T. L. Turner, "A New Thermoelastic Model for Analysis of Shape Memory Alloy Hybrid Composites," *J. of Intell. Matl. Sys. & Stru.*, To Appear May 2001.
13. T. L. Turner, "Experimental Validation of a Thermoelastic Model for SMA Hybrid Composites," *Smart Structures and Materials 2001; Modeling, Signal Processing, and Control in Smart Structures*, SPIE Vol. 4326, Paper No. 4326-24, Newport Beach, CA, 2001.

Table 1: Summary of the thermomechanical properties of the glass-epoxy in principal material coordinates.

Temperature, °C	E_1, GPa	E_2, GPa	ν_{12}	G_{12}, GPa	α_1, με/°C	α_2, με/°C
21.1	49.30	20.00	0.29	9.65	5.22	10.80
26.7	49.30	19.86	0.29	9.58	5.83	13.81
37.8	49.16	19.44	0.29	9.24	6.95	21.02
48.9	49.02	18.96	0.29	8.89	7.22	24.14
60.0	48.82	18.48	0.29	8.55	7.00	24.66
65.6	48.75	18.20	0.29	8.41	6.80	24.28
71.1	48.75	17.79	0.29	8.27	6.62	23.90
82.2	48.68	17.03	0.29	7.93	6.34	22.79
93.3	48.61	16.20	0.29	7.58	6.25	22.00
104.4	48.61	15.31	0.29	6.76	6.39	21.92
115.6	48.54	14.41	0.29	6.00	6.77	22.66
121.1	48.54	14.00	0.29	5.58	6.97	23.33
126.7	48.61	13.45	0.29	5.17	7.18	24.01
137.8	48.68	12.41	0.29	4.27	7.42	25.47
148.9	48.82	11.38	0.29	3.45	7.63	26.28

Table 2: Summary of recovery force and tensile tests performed on the Nitinol ribbon at LMA.

Sample #	Prestrain, %	# of Cycles	Maximum Stress, MPa		Young's Modulus, GPa	
			Cycle 1	Cycle 50	120°C	Ambient
1	1.99	50	429.4	296.0	55.50	22.75
2	3.08	50	533.0	363.3	62.47	25.10
3	3.07	10	517.1	396.3	56.06	24.41
4	4.00	50	586.3	412.7	55.64	24.34
5	3.95	10	579.2	442.1	55.92	24.20
6	N/A	0	N/A	N/A	59.78	14.41

Table 3: Summary of the thermomechanical properties of the Nitinol ribbon as determined by tests at NASA LaRC.

Temperature, °C	Recovery Stress, MPa			E, GPa	α_2, με/°C
	Cycle 2	Cycle 3	Cycle 4		
21.1	0	0	0	27.17	6.61
26.7	2.13	1.28	2.13	24.82	6.61
32.2	7.23	5.53	7.23	22.41	6.61
37.8	16.18	13.20	14.05	20.06	6.61
43.3	31.92	28.95	28.52	25.72	6.61
48.9	70.65	70.23	78.74	31.37	7.24
54.4	135.4	137.9	151.9	36.96	7.87
60.0	192.0	199.6	217.9	42.61	8.50
65.6	240.5	256.6	269.4	48.27	9.11
71.1	297.1	301.8	309.8	54.88	9.74
76.7	341.8	341.8	341.3	61.43	10.37
82.2	374.5	373.7	372.0	64.19	11.00
87.8	402.2	399.2	399.2	63.16	11.00
93.3	425.6	419.2	418.8	62.06	11.00
98.9	449.9	438.8	437.5	63.92	11.00
104.4	469.0	451.6	448.2	65.78	11.00
110.0	481.0	464.8	458.8	67.64	11.00
115.6	491.6	475.8	467.3	69.50	11.00
121.1	500.1	485.6	472.9	71.36	11.00
126.7	508.6	490.3	478.8	70.81	11.00
132.2	515.0	496.7	481.8	70.33	11.00
137.8	520.5	500.5	485.2	69.78	11.00

Temperature, °C	Recovery Stress, MPa			E, GPa	α_2, με/°C
	Cycle 2	Cycle 3	Cycle 4		
143.3	523.5	502.2	487.3	69.29	11.00
148.9	527.8	503.9	490.7	68.74	11.00

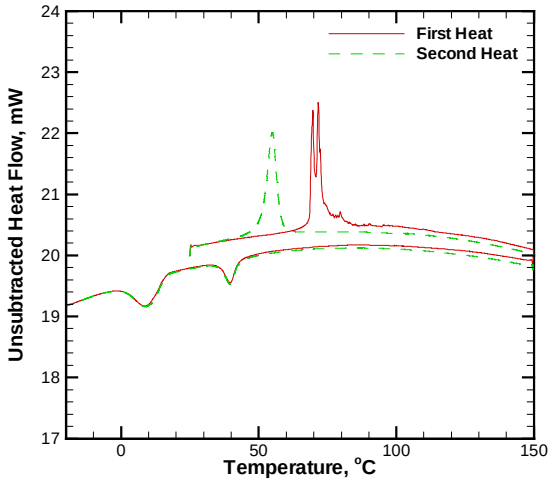

Figure 1: DSC signatures for first- and second-heat of as-received Nitinol material.

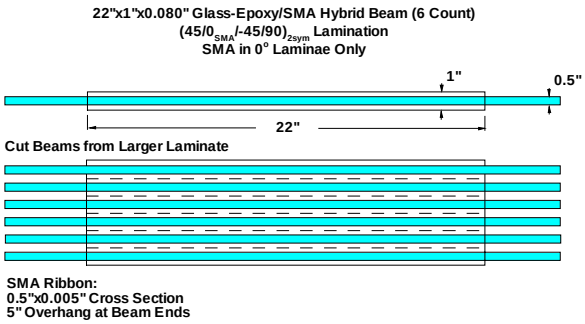

Figure 2: Schematic of beam specimens machined from SMAHC laminate.

Figure 3: Packaging strain recovery rig.

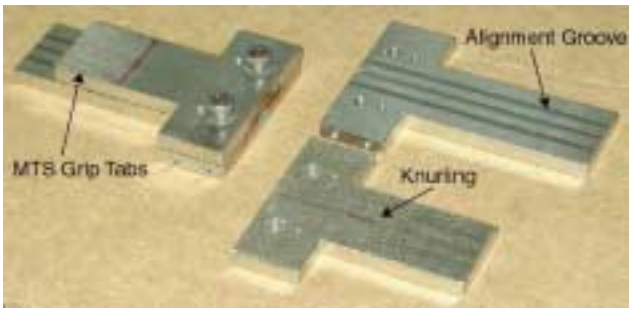

Figure 4: Nitinol gripping apparatus for prestraining and mechanical testing.

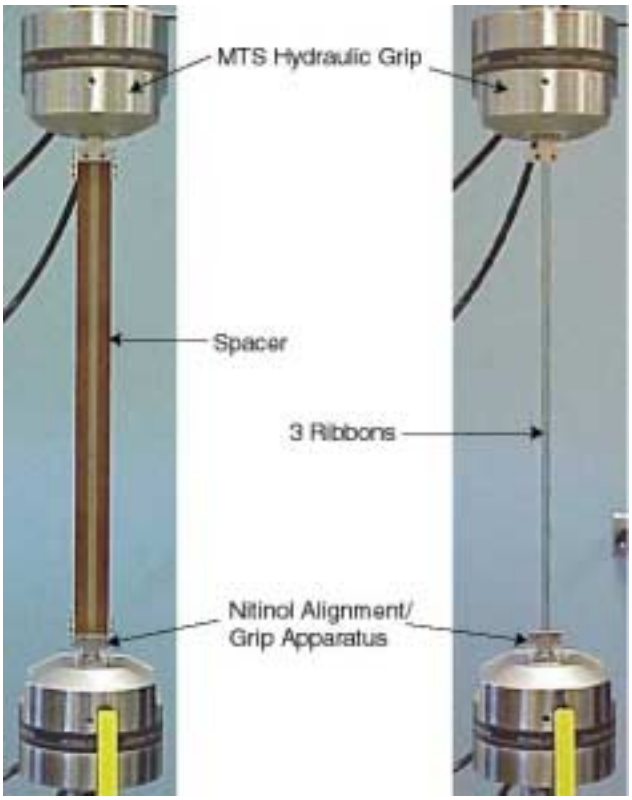

Figure 5: Nitinol ribbon prestrain and mechanical test apparatus.

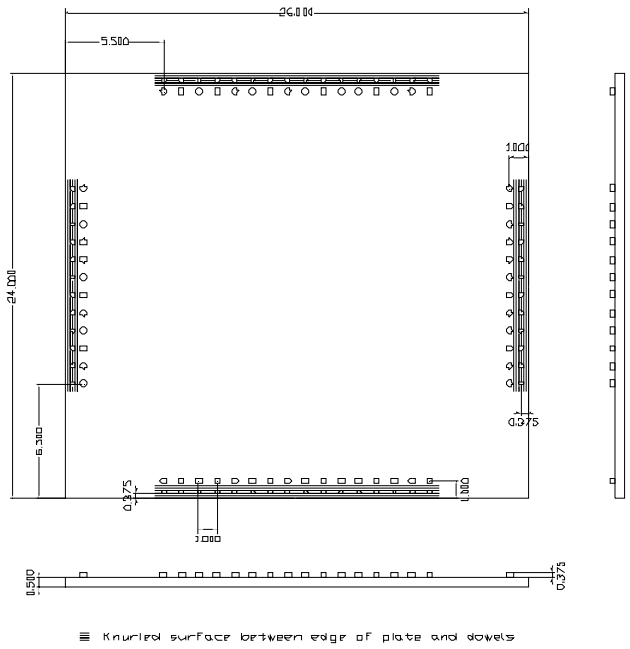

Figure 6: Mechanical drawing of the laminate lay-up and cure tooling apparatus (all dimensions in inches).

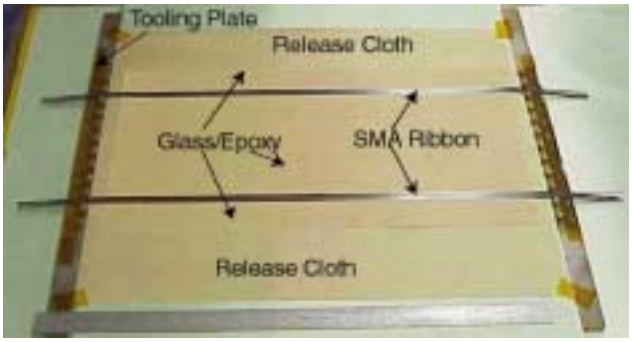

Figure 7: Laminate lay-up procedure at the stage of completing layer 2.

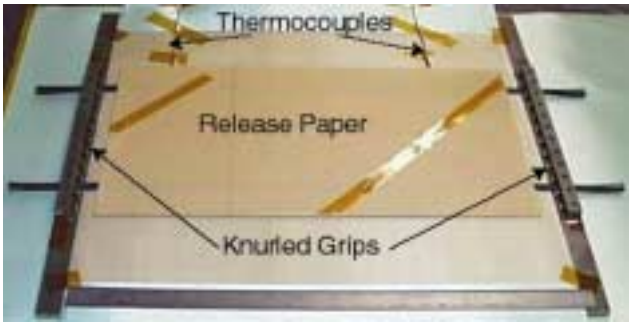

Figure 8: Completed laminate with cure control thermocouples and Nitinol ribbon grips torqued.

Figure 9: Consolidated SMAHC laminated panel.

Figure 10: SMAHC beam specimens.

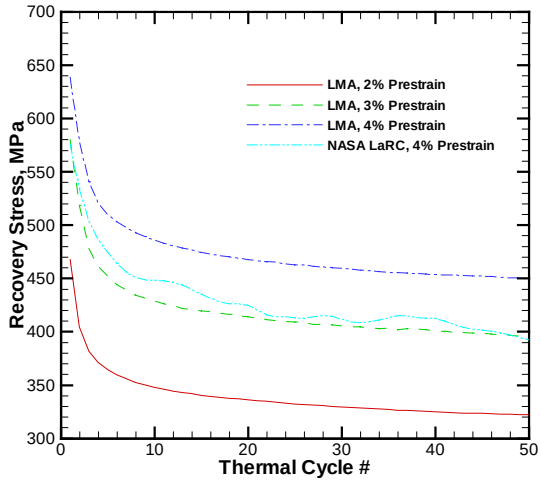

Figure 11: Max recovery stress vs. thermal cycle # for Nitinol samples with 2%, 3% and 4% prestrain.

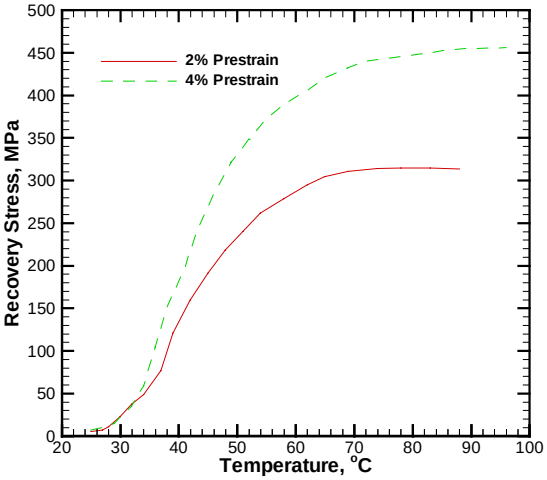

Figure 12: Recovery stress vs. temperature for LMA samples with 2 and 4% prestrain, after 50 thermal cycles.

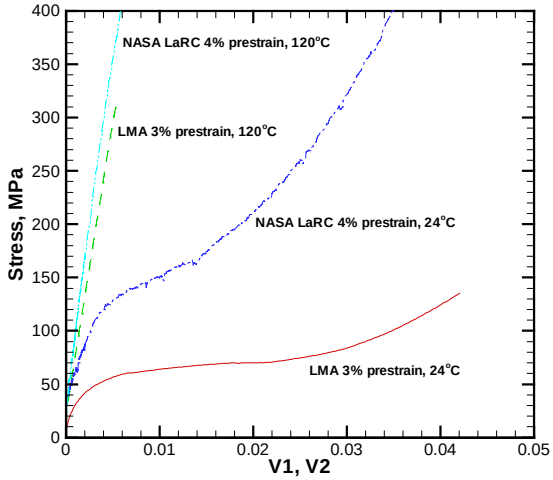

Figure 13: Applied stress vs. strain for LMA 3% and NASA LaRC 4% samples at ambient and 120°C.

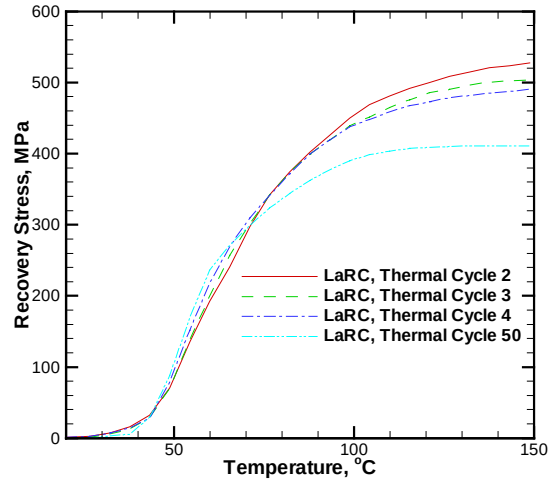

Figure 14: Recovery stress vs. temperature of the NASA LaRC 4% samples for thermal cycles 2–4 and 50.

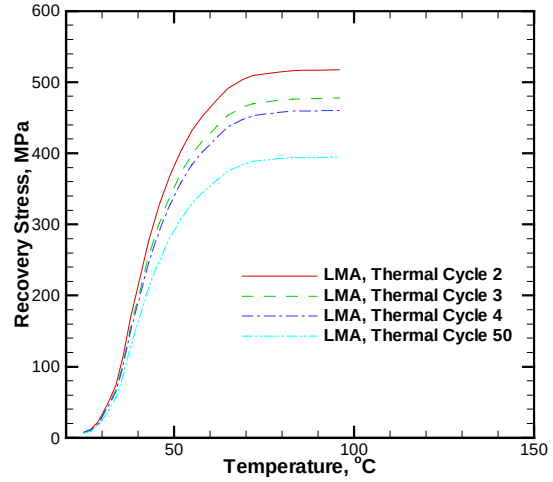

Figure 15: "Constructed" LMA 3% recovery stress vs. temperature for thermal cycles 2–4 and 50.

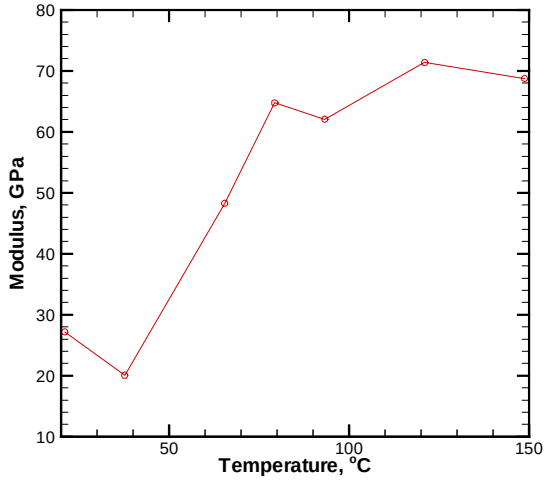

Figure 16: Modulus vs. temperature for the NASA LaRC 4% Nitinol ribbon.

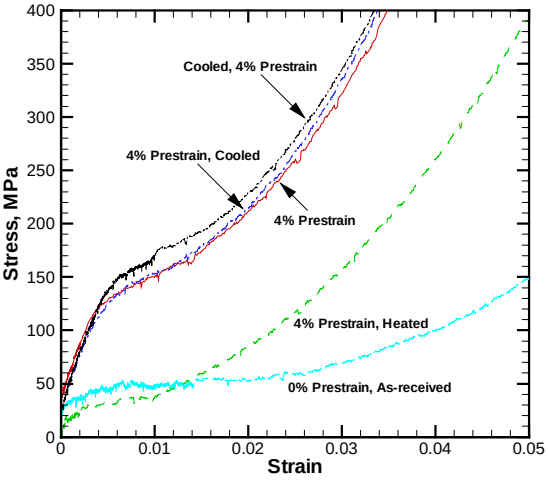

Figure 17: Applied stress vs. strain for a NASA LaRC 4% sample and three other samples with varying processing.